ESO observing programme (title)

VIDEO - The VISTA Deep Extragalactic Observations Survey (ID 179.A-2006, PI: Jarvis)

Abstract

VIDEO is a deep near-infrared survey which targets ~12 square degrees over the ELAIS-S1, XMM-LSS, and E-CDFS extragalactic fields. This document describes the release of all tiles, stacks and the deep stacked data in all areas, VIDEO-ES1, VIDEO-XMM and VIDEO-CDFS in Z,Y,J,H and Ks bands. To the 5σ limit, our band-merged catalogues contain 842,337 unique sources over ~3 deg^2 (two original VIRCAM tiles) in the VIDEO-ES1 area, 1,279,857 unique sources over the ~4.5 deg^2 in the VIDEO-XMM area and 1,138,485 sources over the ~4.5 deg^2 in the VIDEO-CDFS area, respectively.

Overview of Observations

We release all individual stacked paw prints and tiles from 03/11/2009 through to 11/09/2018 (full dataset) and deep-stack images for the VIDEO fields.
The observing strategy, reduction and photometry for individual tiles, source lists and deep-stack data for the VIDEO survey are fully described in the VIDEO Survey paper (Jarvis et al. 2013).

Release Content

We release individual tile/epoch data – both images and catalogues - in all band over the ES1 survey region (Figure 1), the XMM survey region (Figure 2), and the E-CDFS region (Figure 3). These data have all been (re-)pro-cessed using v1.5 of the VISTA reduction pipeline provided by CASU.

Alongside, we release deep-stacked tiles using all survey data in the field in Z,Y,J,H,Ks filters as well as catalogues in all survey fields at full survey depth. The deep-stack images are provided both as stacks of tiles (total of 8x5 images), and as one large mosaic for each field (3x5 images) combining the individual VIRCAM footprints in each field into one large mosaic each, using data taken over the same period. All deep-stack images are matched to the 2MASS WCS.

Further, we provide band-merged object detection catalogues in each survey fields, one catalogue per survey area.
File "video_er7_00h37-043d59_zyjhks_bmCat_644245094403.fits" covers the VIDEO-ES1 field, containing a total of 842,337 unique. Sources are detected according to the SExtractor parameters given on Page 8&9 in each deep-stack image

Similarly, catalogues "video_er7_02h22-004d47_zyjhks_bmCat_644245094401.fits" - covering the full VIDEO-XMM field - and "video_er7_03h32-028d00_zyjhks_bmCat_644245094402.fits" - covering the full VIDEO-CDFS field - contain 1,279,857 and 1,138,485 unique sources, respectively.

These catalogues provide band-merged photometry using each deep-stack image as the detection image, and providing photometry in the other bands. Individual detection catalogues are limited to 5-sigma detections given the magnitude limits specified for the tiles in tables 4, 5 and 6 and are combined into one catalogue afterwards, maintaining uniqueness of sources. We recommend using only those sources with Ks<23.5 for most studies as this gives a completeness of ~90 per cent (Jarvis et al. 2013).
In the band-merged catalogue, columns where the value is "NaN" denote that the object was detected at the position of the detected source with negative flux. This occurs over all apertures and filters for different objects, but is mostly a problem for the larger aperture.

The deep-stacked data are subsequently processed into a release database (VIDEODR7) as described in (see Cross et al. 2012), and available through VSA (surveys.roe.ac.uk/vsa). This database was used to create and prepare the ESO data release.

In addition to tiles and associated source lists, we include stacked individual paw-prints (i.e. paw prints that are made up of the jittered exposures that were used to produce the final deep-stack image for each filter, see Jarvis et al. 2013 for details).
This release therefore provides all stacked paw-prints, single-OB tiles, for all fields, and all have been reprocessed through version 1.5 of the VISTA pipeline and supersede previous releases.

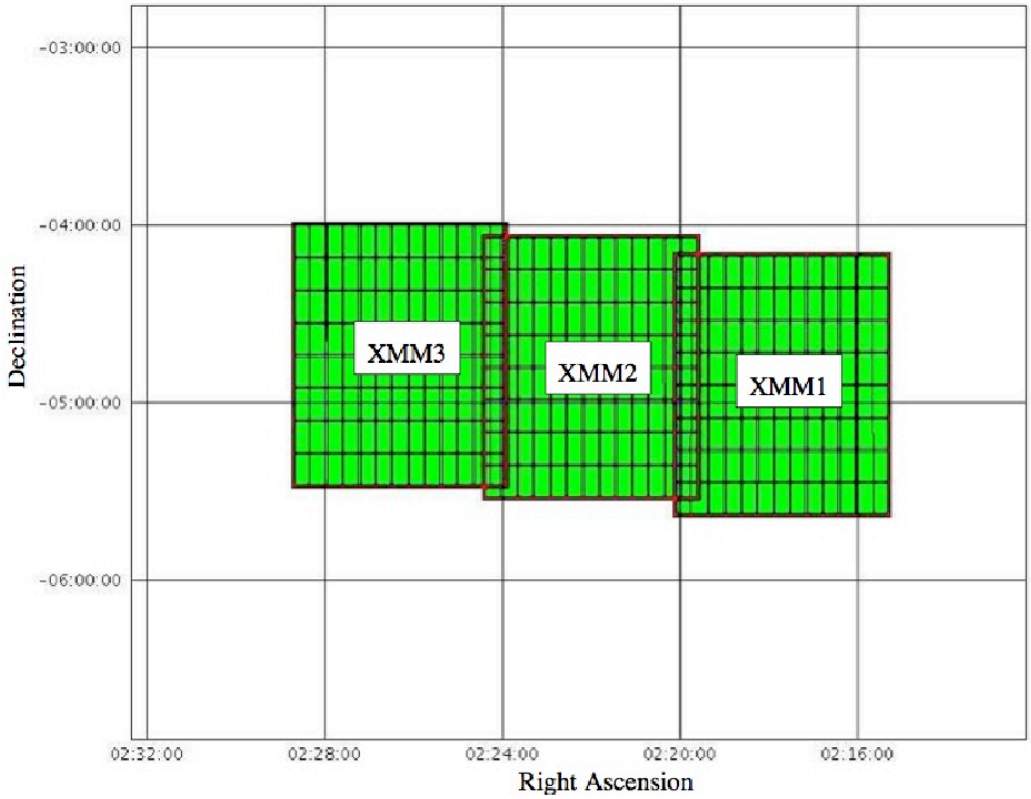

Figure 1: The coordinates of the VIDEO-XMM field. This release is comprised of data over all 3 tiles. Deep stack data are released over all tiles and the complete field, details of which are provided below.

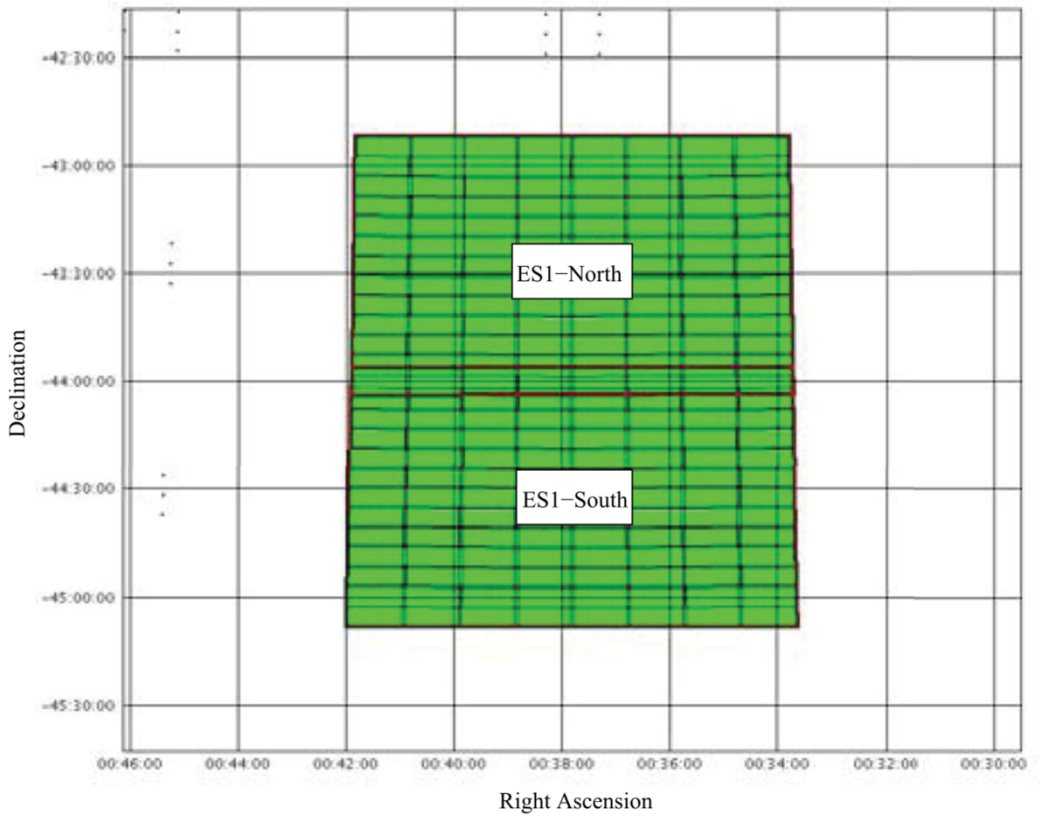

Figure 2: The coordinates of the VIDEO-ES1 field. This release is comprised of data over both tiles. Deep stack data are also released over both tiles and the complete field, details of which are provided below.

Table 1. Summary of deep-stack image and catalogue release and associated dates of observations that contribute to the release.

Tiles	Deep-stack tile filters/catalogues	Deep-stack tile/ catalogues dates	Band-merged catalogue	Band-merged catalogues dates
VIDEO-ES1 = VIDEO-ES1-N & VIDEO-ES1-S	Z,Y,J,H,Ks	07/07/2010-19/10/2017	1 merged catalogue: Z,Y,J,H,Ks	07/07/2010-19/10/2017
VIDEO-XMM = VIDEO-XMM1 & VIDEO-XMM2 & VIDEO-XMM3	Z,Y,J,H,Ks	03/11/2009-07/11/2017	1 merged catalogue: Z,Y,J,H,Ks	03/11/2009-07/11/2017
VIDEO-CDFS = VIDEO-CDFS1 & VIDEO-CDFS2 & VIDEO-CDFS3	Z,Y,J,H,Ks	02/11/2010-11/09/2018	1 merged catalogue: Z,Y,J,H,Ks	02/11/2010-11/09/2018

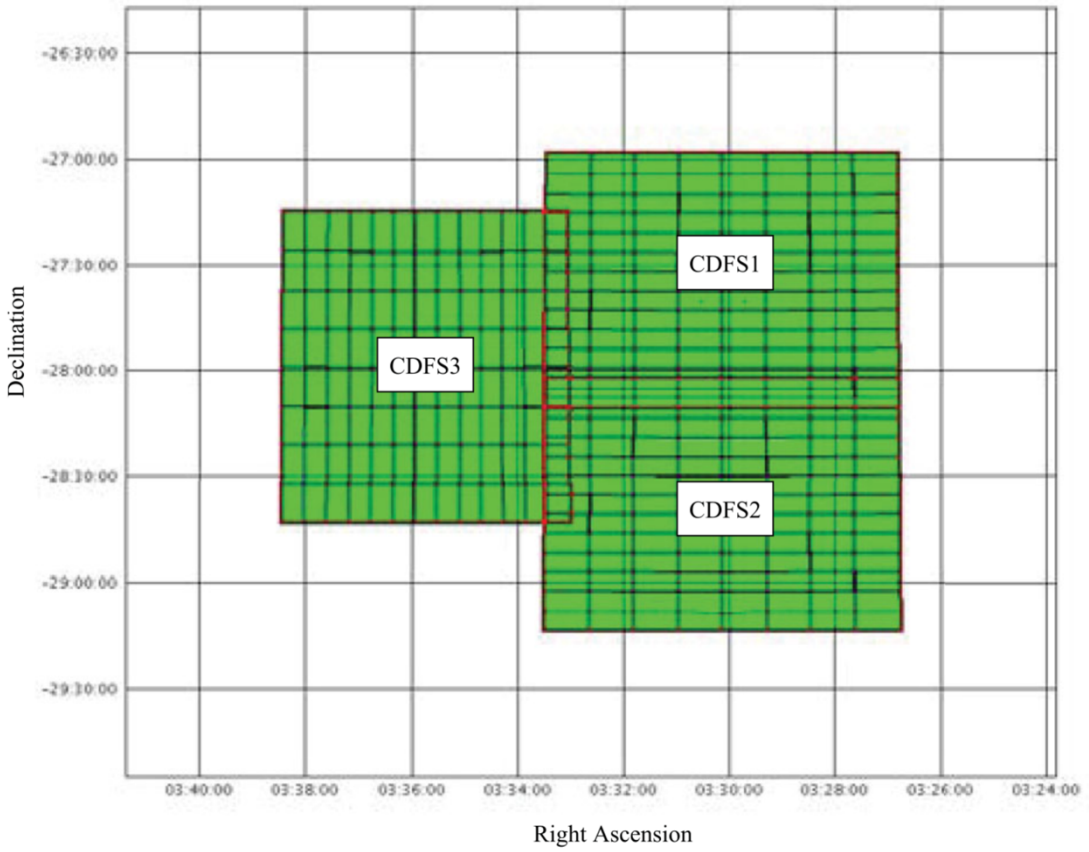

Figure 3: The coordinates of the VIDEO-CDFS field. This release is comprised of data over all 3 tiles. Deep stack data are released over all tiles and the complete field, details of which are provided below.

Table 2. Individual paw-prints released in DR5. Not all of these images are used for the deep stacked tiles released, see Release Notes

Field	Filter	*Integration/pixel*	*Number of paw prints*
VIDEO-ES1-N	Z	450 sec	432
VIDEO-ES1-N	Y	480 sec	684
VIDEO-ES1-N	J	480 sec	247
VIDEO-ES1-N	H	420 sec	313
VIDEO-ES1-N	Ks	420 sec	290
VIDEO-ES1-S	Z	450 sec	266
VIDEO-ES1-S	Y	480 sec	731
VIDEO-ES1-S	J	480 sec	241
VIDEO-ES1-S	H	420 sec	228
VIDEO-ES1-S	Ks	420 sec	267
VIDEO-XMM1	Z	450 sec	448
VIDEO-XMM1	Y	480 sec	646
VIDEO-XMM1	J	480 sec	252
VIDEO-XMM1	H	420 sec	290
VIDEO-XMM1	Ks	420 sec	297
VIDEO-XMM2	Y	480 sec	657
VIDEO-XMM2	J	480 sec	249
VIDEO-XMM2	H	420 sec	240
VIDEO-XMM2	Ks	420 sec	291
VIDEO-XMM3	Z	450 sec	463
VIDEO-XMM3	Y	480 sec	671
VIDEO-XMM3	J	480 sec	232
VIDEO-XMM3	H	420 sec	243
VIDEO-XMM3	Ks	420 sec	311
VIDEO-CDFS1	Z	450 sec	110
VIDEO-CDFS1	Y	480 sec	673
VIDEO-CDFS1	J	480 sec	230
VIDEO-CDFS1	H	420 sec	272
VIDEO-CDFS1	Ks	420 sec	303
VIDEO-CDFS2	Y	480 sec	601
VIDEO-CDFS2	J	480 sec	307
VIDEO-CDFS2	H	420 sec	240
VIDEO-CDFS2	Ks	420 sec	266
VIDEO-CDFS3	Y	480 sec	757
VIDEO-CDFS3	J	480 sec	233
VIDEO-CDFS3	H	420 sec	240
VIDEO-CDFS3	Ks	420 sec	285

Table 3. Number of individual tiles released in DR5.

Field	Filter	*Integration/tile*	*Integration/pixel*	*Number of Tiles*
VIDEO-ES1-N	Z	2700 sec	900 sec	66
VIDEO-ES1-N	Y	2880 sec	960 sec	113
VIDEO-ES1-N	J	2880 sec	960 sec	41
VIDEO-ES1-N	H	2520 sec	840 sec	49
VIDEO-ES1-N	Ks	2520 sec	840 sec	47
VIDEO-ES1-S	Z	2700 sec	900 sec	43
VIDEO-ES1-S	Y	2880 sec	960 sec	121
VIDEO-ES1-S	J	2880 sec	960 sec	40
VIDEO-ES1-S	H	2520 sec	840 sec	37
VIDEO-ES1-S	Ks	2520 sec	840 sec	43
VIDEO-XMM1	Z	2700 sec	900 sec	74
VIDEO-XMM1	Y	2880 sec	960 sec	105
VIDEO-XMM1	J	2880 sec	960 sec	42
VIDEO-XMM1	H	2520 sec	840 sec	48
VIDEO-XMM1	Ks	2520 sec	840 sec	48
VIDEO-XMM2	Y	2880 sec	960 sec	108
VIDEO-XMM2	J	2880 sec	960 sec	39
VIDEO-XMM2	H	2520 sec	840 sec	40
VIDEO-XMM2	Ks	2520 sec	840 sec	48
VIDEO-XMM3	Z	2700 sec	900 sec	74
VIDEO-XMM3	Y	2880 sec	960 sec	111
VIDEO-XMM3	J	2880 sec	960 sec	38
VIDEO-XMM3	H	2520 sec	840 sec	40
VIDEO-XMM3	Ks	2520 sec	840 sec	50
VIDEO-CDFS1	Z	2700 sec	900 sec	17
VIDEO-CDFS1	Y	2880 sec	960 sec	110
VIDEO-CDFS1	J	2880 sec	960 sec	37
VIDEO-CDFS1	H	2520 sec	840 sec	45
VIDEO-CDFS1	Ks	2520 sec	840 sec	49
VIDEO-CDFS2	Y	2880 sec	960 sec	100
VIDEO-CDFS2	J	2880 sec	960 sec	51
VIDEO-CDFS2	H	2520 sec	840 sec	40
VIDEO-CDFS2	Ks	2520 sec	840 sec	44
VIDEO-CDFS3	Y	2880 sec	960 sec	124
VIDEO-CDFS3	J	2880 sec	960 sec	37
VIDEO-CDFS3	H	2520 sec	840 sec	40
VIDEO-CDFS3	Ks	2520 sec	840 sec	47

Table 4. Measured 5σ image depths for the VIDEO-ES1 deep-stack release in 1-5 arcsec diameter apertures in AB magnitudes. The time given is the total integration time of the paw-prints used to measure these values, divided by number of tiles with data at this wavelength. Where times are very different in individual tiles, the numbers are given for each tile. Note that these are different to the ABMAGLIM values given in the headers, which are 5σ limits for point-sources. No data in the Z-band has been taken after 7.1.2013, as it was decided to be more beneficial if the observing time was split up between the other filters, as z-band data is often provided by optical counter-part surveys.

Filter	Average Time (h) Per pixel	1" (5σ)	2" (5σ)	3" (5σ)	4" (5σ)	5" (5σ)
Z	ES1-north: 12.64 ES1-south: 8.25 (average: 10.44)	26.39 26.20 (Avg:26.33)	25.31 25.15 (25.25)	24.65 24.50 (24.60)	24.16 24.04 (24.12)	23.78 23.67 (23.74)
Y	25.4	26.10	25.03	24.38	23.90	23.52
J	9.27	25.56	24.55	23.94	23.50	23.15
H	8.65	25.02	24.00	23.41	22.99	22.66
Ks	9.82	24.70	23.72 ES1-north: 23.74 ES1-south: 23.67	23.15	22.74	22.41

Table 5. See table 4, for VIDEO-XMM field

Filter	Time (h) Per pixel	1" (5σ)	2" (5σ)	3" (5σ)	4" (5σ)	5" (5σ)
Z	17.26 (only XMM1 and XMM3)	26.48	25.39	24.71	24.22	23.82
Y	25.11	26.11	25.04	24.40	23.93	23.55
J	9.78	25.55	24.55	23.95	23.51	23.16
H	8.85	25.07	24.05	23.46	23.04	22.71
Ks	10.11	24.67	23.70 XMM1: 23.62 XMM2: 23.67 XMM3: 23.74	23.13	22.72	22.40

Table 6. See table 4, for VIDEO-CDFS field

Filter	Time (h) Per pixel	1" (5σ)	2" (5σ)	3" (5σ)	4" (5σ)	5" (5σ)
Z	3.89 (only CDFS1)	25.67	24.69	24.11	23.70	23.37
Y	25.21	26.11	25.04	24.40	23.93	23.56
J	10.62	25.52	24.52	23.92	23.49	23.14
H	8.71	25.03	24.03	23.44	23.03	22.70
Ks	9.83	24.59	23.63 CDFS1: 23.65 CDFS2: 23.56 CDFS3: 23.56	23.07	22.67	22.35

Release Notes

Data Reduction and Calibration

Initial data reduction steps are performed at the Cambridge Astronomical Survey Unit (CASU) using a software pipeline developed specifically for the reduction of VIRCAM data, as part of the VISTA Data Flow System described by Irwin et al. (2004) and updated on the CASU webpages. This pipeline is modular, and allows different processing recipes to be applied to data obtained with different observing strategies.

For the VIDEO survey, the following steps are applied to each raw data frame (itself the result of NDIT double-correlated- sampling exposures which are co-added by the data acquisition system):

- De-striping – removes a low-level horizontal stripe pattern introduced by the controller and correlates over the four detectors on each controller,
- linearity correction – corrects for the non-linear detector response which is typically 2-4 per cent depending on the detector,
- dark correction – subtracts a mean dark exposure from the image, correcting for dark current and some other electronic effects,
- flat field correction – divides images by a mean twilight sky image, to correct for position-dependent variations in telescope/camera throughput and detector response,
- sky background correction – subtracts an estimate of the atmospheric emission (more details can be found in Jarvis et al. 2013, MNRAS, 428, 1281),
- astrometric calibration–compares the positions of stars in the image with those in the 2MASS point source catalogue (Skrutskie et al. 2006),
- photometric calibration – calculates magnitudes in the VISTA Vega-magnitude photometric system for unsaturated 2MASS stars in the image using their magnitudes and colours in the 2MASS point source catalogue, to set the zero point in the VISTA photometric system, and
- jitter stacking – combines the jittered images in a single paw- print position, using a mean stack of bi-linearly-resampled images, with outlier rejection to remove cosmic rays, fast-moving objects, and bad pixels.

All individual epoch images and catalogues of this process are being released.

The deep stacked images provided are based on the paw-print data and use only those paw-print images with <0.9 arcsec seeing. As such, parts of completed OBs are not included in the deep stacks, on the other hand some data from aborted OBs are still incorporated in the deep stacks if the individual paw-print met the seeing constraint. Due to the independent data selection for the deep images and the single-OB images, it results for example that the deep co-added images have a total integration time per pixel that is higher than the arithmetic sum of the integration times of the individual Ks tiles.

We further remove paw-prints with incomplete jitter patterns and images with seeing measurements <0.5" from the samples used for the deep stacks, as they have been visually found to be of bad quality, as well as images with saturated background. The latter have been identified by their width/σ of the distribution in sky pixels (3- σ clipped mean/sigma) being above a certain threshold (σ_Z>8.0, σ_Y>6.0, σ_J>12.0, σ_H>15.0, σ_{Ks}>13.0, empirically chosen and verified)

For the source catalogue:

- Source detection was performed separately for each individual filter. For the deep-stack single-band source lists and the band-merged source catalogue, we carry out the detection and measurement of source photometry using SExtractor (Bertin & Arnouts 1996), with the following parameters (see SExtractor documentation for more information):
  - DETECT_MINAREA 3
  - THRESH_TYPE RELATIVE
  - DETECT_THRESH 3
  - ANALYSIS_THRESH 3
  - FILTER Y
  - FILTER_NAME default.conv
  - DEBLEND_NTHRESH 32

- DEBLEND_MINCONT 0.0008
- CLEAN Y
- CLEAN_PARAM 1.0
- MASK_TYPE CORRECT
- PHOT_AUTOPARAMS 2.5, 3.5
- PHOT_PETROPARAMS 2.0, 3.5
- BACK_TYPE AUTO
- BACK_SIZE 64
- BACK_FILTERSIZE 3
- BACKPHOTO_TYPE LOCAL
- BACKPHOTO_THICK 24
- BACK_FILTTHRESH 0.0

- The catalogue is retrospectively limited to 5-sigma detections, using the magnitude limit derived during our analysis.
- Astrometry is referenced to 2MASS in all individual epoch data and the individual epoch catalogues, as well as in one set of the deep stack data.
- Photometry is performed in the Vega system, and is calibrated by reference to 2MASS stars, using the following colour equations (taken from http://casu.ast.cam.ac.uk/surveys-projects/vista/technical/photometric-properties and referenced in González-Fernandéz, et al. 2018):
  - $Z_{VIRCAM} = J_{2MASS} + (0.86 \pm 0.08)*(J-Ks)_{2MASS}$
  - $Y_{VIRCAM} = J_{2MASS} + (0.46 \pm 0.02) *(J-Ks)_{2MASS}$
  - $J_{VIRCAM} = J_{2MASS} - (0.031 \pm 0.006) *(J-Ks)_{2MASS}$
  - $H_{VIRCAM} = H_{2MASS} + (0.015 \pm 0.005) *(J-Ks)_{2MASS}$
  - $Ks_{VIRCAM} = Ks_{2MASS} + (0.006 \pm 0.007) *(J-Ks)_{2MASS}$
- The released catalogue are on the AB magnitude system with the following used to convert from Vega to AB.
  Z(+0.502), Y(+0.600), J(+0.9158), H(+1.3663), Ks(+1.8266)
- No illumination correction has been applied.
- No correction for extinction has been applied. However, extinction is extremely low for these high-galactic-latitude fields.

For the individual tiles the associated tile-specific source lists are created using the CASU VSA pipeline, details of which can be found at http://casu.ast.cam.ac.uk/surveys-projects/vista/technical/tiles.

In order to display and analyse the deep-stack images, which are >2GB, a 64-bit machine is recommended. Then all images can be displayed within ds9 for example. If working on a machine with less RAM, we recommend using the fitscopy utility within cfitsio, which can be used to extract subsections of the images of interest,
e.g. fitscopy 'filename.fits[x1:x2,y1:y2]' filename.trim.fits

Data Quality

- Astrometric checks have been carried out by comparing with the 2MASS stars within the tiled fields. No systematic offsets are found and the rms scatter is found to be ~0.25 arcsec.
- The zero point is uniform across the tile to within the quoted uncertainty (<0.01 mag).
- Photometry has also been checked against unresolved 2MASS sources within the VIDEO field. We find very good agreement between 2MASS and VIDEO after applying the colour equations to move from the 2MASS system to the VIDEO photometric system.
- The fraction of spurious sources, calculated by inverting the tiled image and re-extracting the sources using the same prescription used for the real extraction, is 0.08 per cent for the Ks-band selected catalogue to the 3sigma depth of 23.72 (2 arcsec aperture, see Table 4) in the central part of the ES1 field, avoiding edge effects and with bright stars masked out. Although a similar analysis has not been carried out on the other tiles, we expect a similar contamination rate. Around bright stars and along the image edges, the spurious detections are somewhat more regular.

- Table 3 in Jarvis et al. (2013) provides the completeness for the various filters over the VIDEO-XMM3 deep-stack. Tables 4, 5 and 6 in this document provide similar data for the full VIDEO fields released here.

Known issues

Regions of bad pixels in Detector 1 and time varying quantum efficiency in detector 16 renders these detectors the most problematic. The regions of poorer noise statistics are evident in the confidence images. An offset in the photometric calibration of the Y-band data (of the order of 0.1 mag too bright), was an issue in previous releases, this has now been corrected.

For the both ES1-North and ES1-South tiles the central position was shifted slightly between early observations and the later ones. The tile centre is given by the TL_RA and TL_DEC keywords in the header information and these provide the centre of the given tile.

The XMM2 field (and hence the central part of the XMM field) also contains a region towards the north of the field that is affected by stray light. We identified the source of this stray light to come from Mira, a magnitude 3-9 variable star, which is just over 3 degrees away in the direction of the feature.

Previous Releases

In ES1 field:
The second public data release of the VIDEO programme via the ESO Science Archive Facility, the VIDEO-ES1 Data Release Number 2, Date: 04.04.2014, contained 119 individual (i.e. single-OB) tile images in the VIDEO-ES1-North and ES1-South fields and their associated single-band source lists. In DR3 Date: 26/03/2015, we released a total of 401 individual (single-OB) tile images and the associated single-band source lists that have been processed through version 1.3 of the VISTA pipeline. In DR4 we released 339 paw-prints and 56 tile images and the associated single-band source lists. We also released deep-stack images in both fields created from the individual paw-print images that were also processed through v1.3 of the pipeline.

In XMM field:
The first public data release of the VIDEO programme via the ESO Science Archive Facility, the VIDEO-XMM Data Release Number 1, Date: 25.07.2011, contained 97 individual (i.e. single-OB) tile images in the VIDEO-XMM3 field and their associated single-band source lists. DR2 added 156 single-OB images in the VIDEO-XMM fields 1, 2 and 3. DR2 was also the first release that included deep co-added images of the XMM3 field including the associated single-band source lists and the resulting deep photometric catalogue where the ZYJHKs data had been merged. In DR3 we released a total of 560 individual (single-OB) tile images and the associated single-band source lists that were processed through version 1.3 of the VISTA pipeline. In DR4 we released an additional 531 paw-print files and 88 tiles covering XMM1 and XMM2. We also released deep-stack images in all three fields created from the individual paw-print images that were also processed through v1.3 of the pipeline.

In CDFS field:
The third public data release of the VIDEO programme via the ESO Science Archive Facility, the VIDEO-CDFS Data Release Number 2, Date: 26/02/2015, contained paw-prints and deep stacks in a subset of the filters over the three CDFS tiles. In DR3 we release a total of 743 individual paw-prints (single-OB) and 121 tile images and the associated single-band source lists that have been processed through version 1.3 of the VISTA pipeline. We also released deep-stack images in CDFS1, CDFS2 and CDFS3 created from the individual paw-print images that were also processed through v1.3 of the pipeline.
Although no DR4 has been released in CDFS, this current release is named DR5 to be consistent with the other fields.

In DR5, we release all paw-prints and tiles of the VIDEO survey, as well as deep-stack images in all fields, created from the individual paw-print images. **Previous releases are superseded by this current release of all data, with improved data reduction, processed through v1.5 of the pipeline**.

Data Format

Files Types

Here we release deep-stacked images and associated aperture matched catalogues. The naming convention for these is:
video_er6_$POSITION$_mosaic_$FILTERNAME$_deepimage_$MFID$.fits.fz
video_er6_$POSITION$_mosaic_$FILTERNAME$_deepconf_$MFID$.fits.fz
video_er6_$POSITION$_mosaic_$FILTERNAME$_jpeg_$MFID$.jpg
video_er6_$POSITION$_mosaic_$FILTERNAME$_jpeg_$MFID$.jpg
video_er6_$POSITION$_mosaic_$FILTERNAME$_cat_$MFID$.fits

for deep images from individual tiles and

video_er7_$POSITION$_mosaic_$FILTERNAME$_deepimage_$MFID$.fits.fz
video_er7_$POSITION$_mosaic_$FILTERNAME$_deepconf_$MFID$.fits.fz
video_er7_$POSITION$_mosaic_$FILTERNAME$_jpeg_$MFID$.jpg
video_er7_$POSITION$_mosaic_$FILTERNAME$_jpeg_$MFID$.jpg
video_er7_$POSITION$_mosaic_$FILTERNAME$_cat_$MFID$.fits

for deep images covering each region.

where $POSITION$ is a string like 00h38-45d00 for the ES1 field (exact coordinates depend on the subfield in question), 02h22-04d00 for the XMM field (exact coordinates depend on the subfield in question) and 03h33-28d00 for the XMM field (exact coordinates depend on the subfield in question).
$FILTERNAME$ is z,y,j,h,ks AND $MFID$ is the multiframeID in our database.
We note that the jpg images are provided for a quick-look at both the science frames and the confidence images.

The single-tile images, confidence maps and source lists have the following naming convention:
v$DATE$_OBS_NUMBER_st_tl.fits.fz
v$DATE$_OBS_NUMBER_st_tl_conf.fits.fz
v$DATE$_OBS_NUMBER_st_tl_cat.fits,
for the tiled image, the confidence image and the source list respectively. OBS_NUMBER refers to the final observation number for the individual paw-prints which contribute to the tile.

The paw-print images, confidence maps and source lists have the following naming convention:
v$DATE$_OBS_NUMBER_st.fits.fz
v$DATE$_OBS_NUMBER_st_conf.fits.fz
v$DATE$_OBS_NUMBER_st_cat.fits,
for the tiled image, the confidence image and the source list respectively. OBS_NUMBER refers to the final observation number for the individual paw-prints which contribute to the final paw print.

Catalogue Columns

A complete list of catalogue columns for the single-band deep-stack source catalogues is given in Table 5, and Table 6 gives the columns for the band-merged catalogue. Table 7 gives the column names of the source catalogues derived from individual single tiles derived using the CASU source extraction pipeline (see http://casu.ast.cam.ac.uk/surveys-projects/vista/technical/catalogue-generation).
A brief description of these columns now follows.

Source IDs (ObjID, IAUNAME, SOURCEID)
ObjID gives the unique object identifier for the object in the given filter for this DR. These identifiers are subject to change in individual releases and can hence not be used as inter-release object IDs.
IAUNAME is the source identifier following the IAU convention, and comprising the survey identifier ("VID") and then the (truncated) RA and Dec of each object. SOURCEID is the unique source number for the merged catalogue.

Positional Parameters (X, Y, RA, Dec)
X and Y report the position of the object in pixels on the relevant image (which applies to all the stacks, as they share the same coordinate system). RA and Dec (and RA200 and DEC2000 in the merged catalogue) in equinox J2000 are based on the 2MASS astrometric system as described in Jarvis et al. (2013).

Magnitude measurements and errors
Aperture magnitudes are measured in 2" and 5.7" fixed diameter apertures (APERMAGNOAPERCORR3 and APERMAGNOAPERCORR6 columns). We also supply seeing corrected "real" aperture magnitudes for these apertures (APERMAG3 and APERMAG6 columns) that provide the photometry in a seeing convolved 2 and 5.7" aperture. The uncertainties on aperture magnitudes are given in APERMAG3ERR, APERMAG6ERR, APERMAGNOAPERCORR3 and APERMAGNOAPERCORR6. The Petrosian magnitude and the associated error are also provided in columns denoted PETROMAG and PETROMAGERR respectively. SExtractor MAG_AUTO magnitudes and uncertainties are denoted as AUTOMAG and AUTOMAGERR.

To correct for correlated noise in the images, the errors for fixed aperture photometry are estimated by measuring the RMS flux in randomly placed apertures of the same size, then adding Poisson errors based on object counts. Errors for Petrosian fluxes are corrected by scaling the random (non-Poisson) component of the error (as estimated by SExtractor); the scaling factor is estimated by comparing the median SExtractor error for randomly placed 5 arcsec apertures with the actual standard deviation of fluxes in those apertures.

Object flags and source classifier (ERRBITS, CLASSSTAT, MERGEDCLASS, HALFRAD, EBV)
The SExtractor flag is provided in the column denoted ERRBITS, indicating if an object is blended or has otherwise corrupted measurements. The best possible object sample are those objects which have ERRBITS = 0.
CLASSTAT gives the SExtractor star/galaxy classification statistic, where 0-galaxy and 1-star. The MERGEDCLASS column in the band-merged catalogue is the weighted average of the individual CLASSSTAT parameters for that object.
HALFRAD is the SExtractor measurement of the half-light radius in the given filter.

The galactic reddening E(B-V) is reported at the coordinates of each object in the merged catalogue, computed using the Schlegel et al. (1998) dust maps.

In Jarvis et al. objects were discarded when measuring the completeness and reliability of the catalogues using the HALOFLAG term. This flag does not appear in the released catalogues as such a keyword is subject to interpretation and definition. We encourage potential users of the data to define their own object masks according to their science aims.

Table 7. Complete list of supplied catalogue columns in the deep-stacked single-band catalogues.

Column Number	Column Name	Description
1	OBJID	Unique Source Identifier
2	FILTERID	Filter (1=Z; 2=Y; 3=J; 4=H; 5=Ks)
3	X	X coordinate of detection
4	Y	Y coordinate of detection
5	RA	Right Ascension in Decimal Degrees
6	DEC	Declination in Decimal Degrees
7	APERMAGNOAPERCORR3	Fixed Aperture magnitude (2" diameter", AB)
8	APERMAGNOAPERCORR3ERR	Error in calibrated aperture magnitude 3 (2" diameter", AB)
9	APERMAG3	Aperture magnitude corrected to 2" diameter, AB
10	APERMAG3ERR	Error on Aperture magnitude (2", diameter AB)
11	APERMAGNOAPERCORR6	Fixed Aperture magnitude (5.7" diameter, AB)
12	APERMAGNOAPERCORR6ERR	Error in calibrated aperture magnitude 6 (5.7" diameter", AB)
13	APERMAG6	Aperture magnitude corrected to 5.7" diameter, AB
14	APERMAG6ERR	Error on Aperture magnitude (5.7" diameter), AB
15	AUTOMAG	Extended source magnitude (SExtractor MAG_AUTO)
16	AUTOMAGERR	Extended source mag error (SExtractor MAG_AUTO)
17	HALFRAD	Sextractor Half-light radius
18	PETROMAG	Petrosian Magnitude (AB)
19	PETROMAGERR	Error on Petrosian magnitude
20	ERRBITS	Sextractor Flag
21	CLASSSTAT	Sextractor Star/Galaxy classification (0-galaxy, 1-star)

The individual-tile catalogue format was derived from similar APM/SuperCOSMOS/INTWFC/CIRSI analyses that produced 32 4-byte parameters per detected object. This was first enhanced for WFCAM to an 80 4-byte parameter set to include extra parameters for flux estimation and error estimates, and this has now been further refined for the VIRCAM catalogues. The following tables cover the VIRCAM standard and further processing pipeline output catalogues, where for simplicity all derived parameters are stored as floating point numbers even though some of them are more naturally integers. See http://casu.ast.cam.ac.uk/surveys-projects/vista/technical/catalogue-generation for more information.

Table 8. Complete list of supplied catalogue columns in the merged table video_er7_00h37-043d59_zyjhks_bmCat_644245094403.fits. Other tables provided are equivalent.

Column Number	Column Name	Description
1	IAUNAME	IAU Name (not unique)
2	videoID	Unique identifier of object
3	cuEventID	UID of curation event giving rise to this record
4	ra2000	ICRS Right Ascension of object calibrated using 2MASS
5	dec2000	ICRS Declination of object calibrated using 2MASS
6	cx	unit vector of spherical co-ordinates
7	cy	unit vector of spherical co-ordinates
8	cz	unit vector of spherical co-ordinates
9	htmID	Hierarchical Triangular Mesh (HTM) index 20 deep for equatorial co-ordinates
10	id	ID within each region
11	fieldName	the name of the pointing e.g. B418
12	X_IMAGE	X position of object on all images
13	Y_IMAGE	Y position of object on all images
14	Ks_X_IMAGE	X position of object on Ks image
15	Ks_Y_IMAGE	Y position of object on Ks image
16	Ks_ALPHA_J2000	ICRS Right Ascension of object on Ks image calibrated using 2MASS
17	Ks_DELTA_J2000	ICRS Declination of object on Ks image calibrated using 2MASS
18	Ks_FLAGS	SExtractor flags for Ks image objects
19	Ks_MAG_AUTO	Ks band Kron magnitude
20	Ks_MAGERR_AUTO	Error in Ks band Kron magnitude
21	Ks_MAG_PETRO	Ks band Petrosian magnitude
22	Ks_MAGERR_PETRO	Error in Ks band Petrosian magnitude
23	Ks_MAG_APER_1	Ks band 1 arcsec diameter circular aperture magnitude
24	Ks_MAG_APER_2	Ks band 2 arcsec diameter circular aperture magnitude
25	Ks_MAG_APER_3	Ks band 3 arcsec diameter circular aperture magnitude
26	Ks_MAG_APER_4	Ks band 4 arcsec diameter circular aperture magnitude
27	Ks_MAG_APER_5	Ks band 5 arcsec diameter circular aperture magnitude
28	Ks_MAG_APER_6	Ks band 1.41 arcsec diameter circular aperture magnitude
29	Ks_MAG_APER_7	Ks band 2.83 arcsec diameter circular aperture magnitude
30	Ks_MAG_APER_8	Ks band 5.66 arcsec diameter circular aperture magnitude
31	Ks_MAG_APER_9	Ks band 8 arcsec diameter circular aperture magnitude
32	Ks_MAG_APER_10	Ks band 10 arcsec diameter circular aperture magnitude
33	Ks_MAG_APER_11	Ks band 12 arcsec diameter circular aperture magnitude
34	Ks_MAG_APER_12	Ks band 14 arcsec diameter circular aperture magnitude
35	Ks_MAG_APER_13	Ks band 16 arcsec diameter circular aperture magnitude
36	Ks_MAG_APER_14	Ks band 20 arcsec diameter circular aperture magnitude
37	Ks_MAG_APER_15	Ks band 24 arcsec diameter circular aperture magnitude
38	Ks_MAGERR_APER_1	Error in Ks band 1 arcsec diameter circular aperture magnitude
39	Ks_MAGERR_APER_2	Error in Ks band 2 arcsec diameter circular aperture magnitude

40	Ks_MAGERR_APER_3	Error in Ks band 3 arcsec diameter circular aperture magnitude
41	Ks_MAGERR_APER_4	Error in Ks band 4 arcsec diameter circular aperture magnitude
42	Ks_MAGERR_APER_5	Error in Ks band 5 arcsec diameter circular aperture magnitude
43	Ks_MAGERR_APER_6	Error in Ks band 1.41 arcsec diameter circular aperture magnitude
44	Ks_MAGERR_APER_7	Error in Ks band 2.83 arcsec diameter circular aperture magnitude
45	Ks_MAGERR_APER_8	Error in Ks band 5.66 arcsec diameter circular aperture magnitude
46	Ks_MAGERR_APER_9	Error in Ks band 8 arcsec diameter circular aperture magnitude
47	Ks_MAGERR_APER_10	Error in Ks band 10 arcsec diameter circular aperture magnitude
48	Ks_MAGERR_APER_11	Error in Ks band 12 arcsec diameter circular aperture magnitude
49	Ks_MAGERR_APER_12	Error in Ks band 14 arcsec diameter circular aperture magnitude
50	Ks_MAGERR_APER_13	Error in Ks band 16 arcsec diameter circular aperture magnitude
51	Ks_MAGERR_APER_14	Error in Ks band 20 arcsec diameter circular aperture magnitude
52	Ks_MAGERR_APER_15	Error in Ks band 24 arcsec diameter circular aperture magnitude
53	Ks_FLUX_AUTO	Ks band Kron flux
54	Ks_FLUXERR_AUTO	Error in Ks band Kron flux
55	Ks_FLUX_PETRO	Ks band Petrosian flux
56	Ks_FLUXERR_PETRO	Error in Ks band Petrosian flux
57	Ks_FLUX_APER_1	Ks band 1 arcsec diameter circular aperture flux
58	Ks_FLUX_APER_2	Ks band 2 arcsec diameter circular aperture flux
59	Ks_FLUX_APER_3	Ks band 3 arcsec diameter circular aperture flux
60	Ks_FLUX_APER_4	Ks band 4 arcsec diameter circular aperture flux
61	Ks_FLUX_APER_5	Ks band 5 arcsec diameter circular aperture flux
62	Ks_FLUX_APER_6	Ks band 1.41 arcsec diameter circular aperture flux
63	Ks_FLUX_APER_7	Ks band 2.83 arcsec diameter circular aperture flux
64	Ks_FLUX_APER_8	Ks band 5.66 arcsec diameter circular aperture flux
65	Ks_FLUX_APER_9	Ks band 8 arcsec diameter circular aperture flux
66	Ks_FLUX_APER_10	Ks band 10 arcsec diameter circular aperture flux
67	Ks_FLUX_APER_11	Ks band 12 arcsec diameter circular aperture flux
68	Ks_FLUX_APER_12	Ks band 14 arcsec diameter circular aperture flux
69	Ks_FLUX_APER_13	Ks band 16 arcsec diameter circular aperture flux
70	Ks_FLUX_APER_14	Ks band 20 arcsec diameter circular aperture flux
71	Ks_FLUX_APER_15	Ks band 24 arcsec diameter circular aperture flux
72	Ks_FLUXERR_APER_1	Error in Ks band 1 arcsec diameter circular aperture flux
73	Ks_FLUXERR_APER_2	Error in Ks band 2 arcsec diameter circular aperture flux
74	Ks_FLUXERR_APER_3	Error in Ks band 3 arcsec diameter circular aperture flux
75	Ks_FLUXERR_APER_4	Error in Ks band 4 arcsec diameter circular aperture flux
76	Ks_FLUXERR_APER_5	Error in Ks band 5 arcsec diameter circular aperture flux
77	Ks_FLUXERR_APER_6	Error in Ks band 1.41 arcsec diameter circular aperture flux
78	Ks_FLUXERR_APER_7	Error in Ks band 2.83 arcsec diameter circular aperture flux
79	Ks_FLUXERR_APER_8	Error in Ks band 5.66 arcsec diameter circular aperture flux
80	Ks_FLUXERR_APER_9	Error in Ks band 8 arcsec diameter circular aperture flux
81	Ks_FLUXERR_APER_10	Error in Ks band 10 arcsec diameter circular aperture flux

82	Ks_FLUXERR_APER_11	Error in Ks band 12 arcsec diameter circular aperture flux
83	Ks_FLUXERR_APER_12	Error in Ks band 14 arcsec diameter circular aperture flux
84	Ks_FLUXERR_APER_13	Error in Ks band 16 arcsec diameter circular aperture flux
85	Ks_FLUXERR_APER_14	Error in Ks band 20 arcsec diameter circular aperture flux
86	Ks_FLUXERR_APER_15	Error in Ks band 24 arcsec diameter circular aperture flux
87	Ks_CLASS_STAR	Ks band SExtractor classification statistic
88	H_X_IMAGE	X position of object on H image
89	H_Y_IMAGE	Y position of object on H image
90	H_ALPHA_J2000	ICRS Right Ascension of object on H image calibrated using 2MASS
91	H_DELTA_J2000	ICRS Declination of object on H image calibrated using 2MASS
92	H_FLAGS	SExtractor flags for H image objects
93	H_MAG_AUTO	H band Kron magnitude
94	H_MAGERR_AUTO	Error in H band Kron magnitude
95	H_MAG_PETRO	H band Petrosian magnitude
96	H_MAGERR_PETRO	Error in H band Petrosian magnitude
97	H_MAG_APER_1	H band 1 arcsec diameter circular aperture magnitude
98	H_MAG_APER_2	H band 2 arcsec diameter circular aperture magnitude
99	H_MAG_APER_3	H band 3 arcsec diameter circular aperture magnitude
100	H_MAG_APER_4	H band 4 arcsec diameter circular aperture magnitude
101	H_MAG_APER_5	H band 5 arcsec diameter circular aperture magnitude
102	H_MAG_APER_6	H band 1.41 arcsec diameter circular aperture magnitude
103	H_MAG_APER_7	H band 2.83 arcsec diameter circular aperture magnitude
104	H_MAG_APER_8	H band 5.66 arcsec diameter circular aperture magnitude
105	H_MAG_APER_9	H band 8 arcsec diameter circular aperture magnitude
106	H_MAG_APER_10	H band 10 arcsec diameter circular aperture magnitude
107	H_MAG_APER_11	H band 12 arcsec diameter circular aperture magnitude
108	H_MAG_APER_12	H band 14 arcsec diameter circular aperture magnitude
109	H_MAG_APER_13	H band 16 arcsec diameter circular aperture magnitude
110	H_MAG_APER_14	H band 20 arcsec diameter circular aperture magnitude
111	H_MAG_APER_15	H band 24 arcsec diameter circular aperture magnitude
112	H_MAGERR_APER_1	Error in H band 1 arcsec diameter circular aperture magnitude
113	H_MAGERR_APER_2	Error in H band 2 arcsec diameter circular aperture magnitude
114	H_MAGERR_APER_3	Error in H band 3 arcsec diameter circular aperture magnitude
115	H_MAGERR_APER_4	Error in H band 4 arcsec diameter circular aperture magnitude
116	H_MAGERR_APER_5	Error in H band 5 arcsec diameter circular aperture magnitude
117	H_MAGERR_APER_6	Error in H band 1.41 arcsec diameter circular aperture magnitude
118	H_MAGERR_APER_7	Error in H band 2.83 arcsec diameter circular aperture magnitude
119	H_MAGERR_APER_8	Error in H band 5.66 arcsec diameter circular aperture magnitude
120	H_MAGERR_APER_9	Error in H band 8 arcsec diameter circular aperture magnitude
121	H_MAGERR_APER_10	Error in H band 10 arcsec diameter circular aperture magnitude
122	H_MAGERR_APER_11	Error in H band 12 arcsec diameter circular aperture magnitude
123	H_MAGERR_APER_12	Error in H band 14 arcsec diameter circular aperture magnitude
124	H_MAGERR_APER_13	Error in H band 16 arcsec diameter circular aperture magnitude

125	H_MAGERR_APER_14	Error in H band 20 arcsec diameter circular aperture magnitude
126	H_MAGERR_APER_15	Error in H band 24 arcsec diameter circular aperture magnitude
127	H_FLUX_AUTO	H band Kron flux
128	H_FLUXERR_AUTO	Error in H band Kron flux
129	H_FLUX_PETRO	H band Petrosian flux
130	H_FLUXERR_PETRO	Error in H band Petrosian flux
131	H_FLUX_APER_1	H band 1 arcsec diameter circular aperture flux
132	H_FLUX_APER_2	H band 2 arcsec diameter circular aperture flux
133	H_FLUX_APER_3	H band 3 arcsec diameter circular aperture flux
134	H_FLUX_APER_4	H band 4 arcsec diameter circular aperture flux
135	H_FLUX_APER_5	H band 5 arcsec diameter circular aperture flux
136	H_FLUX_APER_6	H band 1.41 arcsec diameter circular aperture flux
137	H_FLUX_APER_7	H band 2.83 arcsec diameter circular aperture flux
138	H_FLUX_APER_8	H band 5.66 arcsec diameter circular aperture flux
139	H_FLUX_APER_9	H band 8 arcsec diameter circular aperture flux
140	H_FLUX_APER_10	H band 10 arcsec diameter circular aperture flux
141	H_FLUX_APER_11	H band 12 arcsec diameter circular aperture flux
142	H_FLUX_APER_12	H band 14 arcsec diameter circular aperture flux
143	H_FLUX_APER_13	H band 16 arcsec diameter circular aperture flux
144	H_FLUX_APER_14	H band 20 arcsec diameter circular aperture flux
145	H_FLUX_APER_15	H band 24 arcsec diameter circular aperture flux
146	H_FLUXERR_APER_1	Error in H band 1 arcsec diameter circular aperture flux
147	H_FLUXERR_APER_2	Error in H band 2 arcsec diameter circular aperture flux
148	H_FLUXERR_APER_3	Error in H band 3 arcsec diameter circular aperture flux
149	H_FLUXERR_APER_4	Error in H band 4 arcsec diameter circular aperture flux
150	H_FLUXERR_APER_5	Error in H band 5 arcsec diameter circular aperture flux
151	H_FLUXERR_APER_6	Error in H band 1.41 arcsec diameter circular aperture flux
152	H_FLUXERR_APER_7	Error in H band 2.83 arcsec diameter circular aperture flux
153	H_FLUXERR_APER_8	Error in H band 5.66 arcsec diameter circular aperture flux
154	H_FLUXERR_APER_9	Error in H band 8 arcsec diameter circular aperture flux
155	H_FLUXERR_APER_10	Error in H band 10 arcsec diameter circular aperture flux
156	H_FLUXERR_APER_11	Error in H band 12 arcsec diameter circular aperture flux
157	H_FLUXERR_APER_12	Error in H band 14 arcsec diameter circular aperture flux
158	H_FLUXERR_APER_13	Error in H band 16 arcsec diameter circular aperture flux
159	H_FLUXERR_APER_14	Error in H band 20 arcsec diameter circular aperture flux
160	H_FLUXERR_APER_15	Error in H band 24 arcsec diameter circular aperture flux
161	H_CLASS_STAR	H band SExtractor classification statistic
162	J_X_IMAGE	X position of object on J image
163	J_Y_IMAGE	Y position of object on J image
164	J_ALPHA_J2000	ICRS Right Ascension of object on J image calibrated using 2MASS
165	J_DELTA_J2000	ICRS Declination of object on J image calibrated using 2MASS
166	J_FLAGS	SExtractor flags for J image objects
167	J_MAG_AUTO	J band Kron magnitude
168	J_MAGERR_AUTO	Error in J band Kron magnitude

169	J_MAG_PETRO	J band Petrosian magnitude
170	J_MAGERR_PETRO	Error in J band Petrosian magnitude
171	J_MAG_APER_1	J band 1 arcsec diameter circular aperture magnitude
172	J_MAG_APER_2	J band 2 arcsec diameter circular aperture magnitude
173	J_MAG_APER_3	J band 3 arcsec diameter circular aperture magnitude
174	J_MAG_APER_4	J band 4 arcsec diameter circular aperture magnitude
175	J_MAG_APER_5	J band 5 arcsec diameter circular aperture magnitude
176	J_MAG_APER_6	J band 1.41 arcsec diameter circular aperture magnitude
177	J_MAG_APER_7	J band 2.83 arcsec diameter circular aperture magnitude
178	J_MAG_APER_8	J band 5.66 arcsec diameter circular aperture magnitude
179	J_MAG_APER_9	J band 8 arcsec diameter circular aperture magnitude
180	J_MAG_APER_10	J band 10 arcsec diameter circular aperture magnitude
181	J_MAG_APER_11	J band 12 arcsec diameter circular aperture magnitude
182	J_MAG_APER_12	J band 14 arcsec diameter circular aperture magnitude
183	J_MAG_APER_13	J band 16 arcsec diameter circular aperture magnitude
184	J_MAG_APER_14	J band 20 arcsec diameter circular aperture magnitude
185	J_MAG_APER_15	J band 24 arcsec diameter circular aperture magnitude
186	J_MAGERR_APER_1	Error in J band 1 arcsec diameter circular aperture magnitude
187	J_MAGERR_APER_2	Error in J band 2 arcsec diameter circular aperture magnitude
188	J_MAGERR_APER_3	Error in J band 3 arcsec diameter circular aperture magnitude
189	J_MAGERR_APER_4	Error in J band 4 arcsec diameter circular aperture magnitude
190	J_MAGERR_APER_5	Error in J band 5 arcsec diameter circular aperture magnitude
191	J_MAGERR_APER_6	Error in J band 1.41 arcsec diameter circular aperture magnitude
192	J_MAGERR_APER_7	Error in J band 2.83 arcsec diameter circular aperture magnitude
193	J_MAGERR_APER_8	Error in J band 5.66 arcsec diameter circular aperture magnitude
194	J_MAGERR_APER_9	Error in J band 8 arcsec diameter circular aperture magnitude
195	J_MAGERR_APER_10	Error in J band 10 arcsec diameter circular aperture magnitude
196	J_MAGERR_APER_11	Error in J band 12 arcsec diameter circular aperture magnitude
197	J_MAGERR_APER_12	Error in J band 14 arcsec diameter circular aperture magnitude
198	J_MAGERR_APER_13	Error in J band 16 arcsec diameter circular aperture magnitude
199	J_MAGERR_APER_14	Error in J band 20 arcsec diameter circular aperture magnitude
200	J_MAGERR_APER_15	Error in J band 24 arcsec diameter circular aperture magnitude
201	J_FLUX_AUTO	J band Kron flux
202	J_FLUXERR_AUTO	Error in J band Kron flux
203	J_FLUX_PETRO	J band Petrosian flux
204	J_FLUXERR_PETRO	Error in J band Petrosian flux
205	J_FLUX_APER_1	J band 1 arcsec diameter circular aperture flux
206	J_FLUX_APER_2	J band 2 arcsec diameter circular aperture flux
207	J_FLUX_APER_3	J band 3 arcsec diameter circular aperture flux
208	J_FLUX_APER_4	J band 4 arcsec diameter circular aperture flux
209	J_FLUX_APER_5	J band 5 arcsec diameter circular aperture flux
210	J_FLUX_APER_6	J band 1.41 arcsec diameter circular aperture flux
211	J_FLUX_APER_7	J band 2.83 arcsec diameter circular aperture flux
212	J_FLUX_APER_8	J band 5.66 arcsec diameter circular aperture flux

213	J_FLUX_APER_9	J band 8 arcsec diameter circular aperture flux
214	J_FLUX_APER_10	J band 10 arcsec diameter circular aperture flux
215	J_FLUX_APER_11	J band 12 arcsec diameter circular aperture flux
216	J_FLUX_APER_12	J band 14 arcsec diameter circular aperture flux
217	J_FLUX_APER_13	J band 16 arcsec diameter circular aperture flux
218	J_FLUX_APER_14	J band 20 arcsec diameter circular aperture flux
219	J_FLUX_APER_15	J band 24 arcsec diameter circular aperture flux
220	J_FLUXERR_APER_1	Error in J band 1 arcsec diameter circular aperture flux
221	J_FLUXERR_APER_2	Error in J band 2 arcsec diameter circular aperture flux
222	J_FLUXERR_APER_3	Error in J band 3 arcsec diameter circular aperture flux
223	J_FLUXERR_APER_4	Error in J band 4 arcsec diameter circular aperture flux
224	J_FLUXERR_APER_5	Error in J band 5 arcsec diameter circular aperture flux
225	J_FLUXERR_APER_6	Error in J band 1.41 arcsec diameter circular aperture flux
226	J_FLUXERR_APER_7	Error in J band 2.83 arcsec diameter circular aperture flux
227	J_FLUXERR_APER_8	Error in J band 5.66 arcsec diameter circular aperture flux
228	J_FLUXERR_APER_9	Error in J band 8 arcsec diameter circular aperture flux
229	J_FLUXERR_APER_10	Error in J band 10 arcsec diameter circular aperture flux
230	J_FLUXERR_APER_11	Error in J band 12 arcsec diameter circular aperture flux
231	J_FLUXERR_APER_12	Error in J band 14 arcsec diameter circular aperture flux
232	J_FLUXERR_APER_13	Error in J band 16 arcsec diameter circular aperture flux
233	J_FLUXERR_APER_14	Error in J band 20 arcsec diameter circular aperture flux
234	J_FLUXERR_APER_15	Error in J band 24 arcsec diameter circular aperture flux
235	J_CLASS_STAR	J band SExtractor classification statistic
236	Y_X_IMAGE	X position of object on Y image
237	Y_Y_IMAGE	Y position of object on Y image
238	Y_ALPHA_J2000	ICRS Right Ascension of object on Y image calibrated using 2MASS
239	Y_DELTA_J2000	ICRS Declination of object on Y image calibrated using 2MASS
240	Y_FLAGS	SExtractor flags for Y image objects
241	Y_MAG_AUTO	Y band Kron magnitude
242	Y_MAGERR_AUTO	Error in Y band Kron magnitude
243	Y_MAG_PETRO	Y band Petrosian magnitude
244	Y_MAGERR_PETRO	Error in Y band Petrosian magnitude
245	Y_MAG_APER_1	Y band 1 arcsec diameter circular aperture magnitude
246	Y_MAG_APER_2	Y band 2 arcsec diameter circular aperture magnitude
247	Y_MAG_APER_3	Y band 3 arcsec diameter circular aperture magnitude
248	Y_MAG_APER_4	Y band 4 arcsec diameter circular aperture magnitude
249	Y_MAG_APER_5	Y band 5 arcsec diameter circular aperture magnitude
250	Y_MAG_APER_6	Y band 1.41 arcsec diameter circular aperture magnitude
251	Y_MAG_APER_7	Y band 2.83 arcsec diameter circular aperture magnitude
252	Y_MAG_APER_8	Y band 5.66 arcsec diameter circular aperture magnitude
253	Y_MAG_APER_9	Y band 8 arcsec diameter circular aperture magnitude
254	Y_MAG_APER_10	Y band 10 arcsec diameter circular aperture magnitude
255	Y_MAG_APER_11	Y band 12 arcsec diameter circular aperture magnitude

256	Y_MAG_APER_12	Y band 14 arcsec diameter circular aperture magnitude
257	Y_MAG_APER_13	Y band 16 arcsec diameter circular aperture magnitude
258	Y_MAG_APER_14	Y band 20 arcsec diameter circular aperture magnitude
259	Y_MAG_APER_15	Y band 24 arcsec diameter circular aperture magnitude
260	Y_MAGERR_APER_1	Error in Y band 1 arcsec diameter circular aperture magnitude
261	Y_MAGERR_APER_2	Error in Y band 2 arcsec diameter circular aperture magnitude
262	Y_MAGERR_APER_3	Error in Y band 3 arcsec diameter circular aperture magnitude
263	Y_MAGERR_APER_4	Error in Y band 4 arcsec diameter circular aperture magnitude
264	Y_MAGERR_APER_5	Error in Y band 5 arcsec diameter circular aperture magnitude
265	Y_MAGERR_APER_6	Error in Y band 1.41 arcsec diameter circular aperture magnitude
266	Y_MAGERR_APER_7	Error in Y band 2.83 arcsec diameter circular aperture magnitude
267	Y_MAGERR_APER_8	Error in Y band 5.66 arcsec diameter circular aperture magnitude
268	Y_MAGERR_APER_9	Error in Y band 8 arcsec diameter circular aperture magnitude
269	Y_MAGERR_APER_10	Error in Y band 10 arcsec diameter circular aperture magnitude
270	Y_MAGERR_APER_11	Error in Y band 12 arcsec diameter circular aperture magnitude
271	Y_MAGERR_APER_12	Error in Y band 14 arcsec diameter circular aperture magnitude
272	Y_MAGERR_APER_13	Error in Y band 16 arcsec diameter circular aperture magnitude
273	Y_MAGERR_APER_14	Error in Y band 20 arcsec diameter circular aperture magnitude
274	Y_MAGERR_APER_15	Error in Y band 24 arcsec diameter circular aperture magnitude
275	Y_FLUX_AUTO	Y band Kron flux
276	Y_FLUXERR_AUTO	Error in Y band Kron flux
277	Y_FLUX_PETRO	Y band Petrosian flux
278	Y_FLUXERR_PETRO	Error in Y band Petrosian flux
279	Y_FLUX_APER_1	Y band 1 arcsec diameter circular aperture flux
280	Y_FLUX_APER_2	Y band 2 arcsec diameter circular aperture flux
281	Y_FLUX_APER_3	Y band 3 arcsec diameter circular aperture flux
282	Y_FLUX_APER_4	Y band 4 arcsec diameter circular aperture flux
283	Y_FLUX_APER_5	Y band 5 arcsec diameter circular aperture flux
284	Y_FLUX_APER_6	Y band 1.41 arcsec diameter circular aperture flux
285	Y_FLUX_APER_7	Y band 2.83 arcsec diameter circular aperture flux
286	Y_FLUX_APER_8	Y band 5.66 arcsec diameter circular aperture flux
287	Y_FLUX_APER_9	Y band 8 arcsec diameter circular aperture flux
288	Y_FLUX_APER_10	Y band 10 arcsec diameter circular aperture flux
289	Y_FLUX_APER_11	Y band 12 arcsec diameter circular aperture flux
290	Y_FLUX_APER_12	Y band 14 arcsec diameter circular aperture flux
291	Y_FLUX_APER_13	Y band 16 arcsec diameter circular aperture flux
292	Y_FLUX_APER_14	Y band 20 arcsec diameter circular aperture flux
293	Y_FLUX_APER_15	Y band 24 arcsec diameter circular aperture flux
294	Y_FLUXERR_APER_1	Error in Y band 1 arcsec diameter circular aperture flux
295	Y_FLUXERR_APER_2	Error in Y band 2 arcsec diameter circular aperture flux
296	Y_FLUXERR_APER_3	Error in Y band 3 arcsec diameter circular aperture flux
297	Y_FLUXERR_APER_4	Error in Y band 4 arcsec diameter circular aperture flux
298	Y_FLUXERR_APER_5	Error in Y band 5 arcsec diameter circular aperture flux
299	Y_FLUXERR_APER_6	Error in Y band 1.41 arcsec diameter circular aperture flux

300	Y_FLUXERR_APER_7	Error in Y band 2.83 arcsec diameter circular aperture flux
301	Y_FLUXERR_APER_8	Error in Y band 5.66 arcsec diameter circular aperture flux
302	Y_FLUXERR_APER_9	Error in Y band 8 arcsec diameter circular aperture flux
303	Y_FLUXERR_APER_10	Error in Y band 10 arcsec diameter circular aperture flux
304	Y_FLUXERR_APER_11	Error in Y band 12 arcsec diameter circular aperture flux
305	Y_FLUXERR_APER_12	Error in Y band 14 arcsec diameter circular aperture flux
306	Y_FLUXERR_APER_13	Error in Y band 16 arcsec diameter circular aperture flux
307	Y_FLUXERR_APER_14	Error in Y band 20 arcsec diameter circular aperture flux
308	Y_FLUXERR_APER_15	Error in Y band 24 arcsec diameter circular aperture flux
309	Y_CLASS_STAR	Y band SExtractor classification statistic
310	Z_X_IMAGE	X position of object on Z image
311	Z_Y_IMAGE	Y position of object on Z image
312	Z_ALPHA_J2000	ICRS Right Ascension of object on Z image calibrated using 2MASS
313	Z_DELTA_J2000	ICRS Declination of object on Z image calibrated using 2MASS
314	Z_FLAGS	SExtractor flags for Z image objects
315	Z_MAG_AUTO	Z band Kron magnitude
316	Z_MAGERR_AUTO	Error in Z band Kron magnitude
317	Z_MAG_PETRO	Z band Petrosian magnitude
318	Z_MAGERR_PETRO	Error in Z band Petrosian magnitude
319	Z_MAG_APER_1	Z band 1 arcsec diameter circular aperture magnitude
320	Z_MAG_APER_2	Z band 2 arcsec diameter circular aperture magnitude
321	Z_MAG_APER_3	Z band 3 arcsec diameter circular aperture magnitude
322	Z_MAG_APER_4	Z band 4 arcsec diameter circular aperture magnitude
323	Z_MAG_APER_5	Z band 5 arcsec diameter circular aperture magnitude
324	Z_MAG_APER_6	Z band 1.41 arcsec diameter circular aperture magnitude
325	Z_MAG_APER_7	Z band 2.83 arcsec diameter circular aperture magnitude
326	Z_MAG_APER_8	Z band 5.66 arcsec diameter circular aperture magnitude
327	Z_MAG_APER_9	Z band 8 arcsec diameter circular aperture magnitude
328	Z_MAG_APER_10	Z band 10 arcsec diameter circular aperture magnitude
329	Z_MAG_APER_11	Z band 12 arcsec diameter circular aperture magnitude
330	Z_MAG_APER_12	Z band 14 arcsec diameter circular aperture magnitude
331	Z_MAG_APER_13	Z band 16 arcsec diameter circular aperture magnitude
332	Z_MAG_APER_14	Z band 20 arcsec diameter circular aperture magnitude
333	Z_MAG_APER_15	Z band 24 arcsec diameter circular aperture magnitude
334	Z_MAGERR_APER_1	Error in Z band 1 arcsec diameter circular aperture magnitude
335	Z_MAGERR_APER_2	Error in Z band 2 arcsec diameter circular aperture magnitude
336	Z_MAGERR_APER_3	Error in Z band 3 arcsec diameter circular aperture magnitude
337	Z_MAGERR_APER_4	Error in Z band 4 arcsec diameter circular aperture magnitude
338	Z_MAGERR_APER_5	Error in Z band 5 arcsec diameter circular aperture magnitude
339	Z_MAGERR_APER_6	Error in Z band 1.41 arcsec diameter circular aperture magnitude
340	Z_MAGERR_APER_7	Error in Z band 2.83 arcsec diameter circular aperture magnitude
341	Z_MAGERR_APER_8	Error in Z band 5.66 arcsec diameter circular aperture magnitude
342	Z_MAGERR_APER_9	Error in Z band 8 arcsec diameter circular aperture magnitude

343	Z_MAGERR_APER_10	Error in Z band 10 arcsec diameter circular aperture magnitude
344	Z_MAGERR_APER_11	Error in Z band 12 arcsec diameter circular aperture magnitude
345	Z_MAGERR_APER_12	Error in Z band 14 arcsec diameter circular aperture magnitude
346	Z_MAGERR_APER_13	Error in Z band 16 arcsec diameter circular aperture magnitude
347	Z_MAGERR_APER_14	Error in Z band 20 arcsec diameter circular aperture magnitude
348	Z_MAGERR_APER_15	Error in Z band 24 arcsec diameter circular aperture magnitude
349	Z_FLUX_AUTO	Z band Kron flux
350	Z_FLUXERR_AUTO	Error in Z band Kron flux
351	Z_FLUX_PETRO	Z band Petrosian flux
352	Z_FLUXERR_PETRO	Error in Z band Petrosian flux
353	Z_FLUX_APER_1	Z band 1 arcsec diameter circular aperture flux
354	Z_FLUX_APER_2	Z band 2 arcsec diameter circular aperture flux
355	Z_FLUX_APER_3	Z band 3 arcsec diameter circular aperture flux
356	Z_FLUX_APER_4	Z band 4 arcsec diameter circular aperture flux
357	Z_FLUX_APER_5	Z band 5 arcsec diameter circular aperture flux
358	Z_FLUX_APER_6	Z band 1.41 arcsec diameter circular aperture flux
359	Z_FLUX_APER_7	Z band 2.83 arcsec diameter circular aperture flux
360	Z_FLUX_APER_8	Z band 5.66 arcsec diameter circular aperture flux
361	Z_FLUX_APER_9	Z band 8 arcsec diameter circular aperture flux
362	Z_FLUX_APER_10	Z band 10 arcsec diameter circular aperture flux
363	Z_FLUX_APER_11	Z band 12 arcsec diameter circular aperture flux
364	Z_FLUX_APER_12	Z band 14 arcsec diameter circular aperture flux
365	Z_FLUX_APER_13	Z band 16 arcsec diameter circular aperture flux
366	Z_FLUX_APER_14	Z band 20 arcsec diameter circular aperture flux
367	Z_FLUX_APER_15	Z band 24 arcsec diameter circular aperture flux
368	Z_FLUXERR_APER_1	Error in Z band 1 arcsec diameter circular aperture flux
369	Z_FLUXERR_APER_2	Error in Z band 2 arcsec diameter circular aperture flux
370	Z_FLUXERR_APER_3	Error in Z band 3 arcsec diameter circular aperture flux
371	Z_FLUXERR_APER_4	Error in Z band 4 arcsec diameter circular aperture flux
372	Z_FLUXERR_APER_5	Error in Z band 5 arcsec diameter circular aperture flux
373	Z_FLUXERR_APER_6	Error in Z band 1.41 arcsec diameter circular aperture flux
374	Z_FLUXERR_APER_7	Error in Z band 2.83 arcsec diameter circular aperture flux
375	Z_FLUXERR_APER_8	Error in Z band 5.66 arcsec diameter circular aperture flux
376	Z_FLUXERR_APER_9	Error in Z band 8 arcsec diameter circular aperture flux
377	Z_FLUXERR_APER_10	Error in Z band 10 arcsec diameter circular aperture flux
378	Z_FLUXERR_APER_11	Error in Z band 12 arcsec diameter circular aperture flux
379	Z_FLUXERR_APER_12	Error in Z band 14 arcsec diameter circular aperture flux
380	Z_FLUXERR_APER_13	Error in Z band 16 arcsec diameter circular aperture flux
381	Z_FLUXERR_APER_14	Error in Z band 20 arcsec diameter circular aperture flux
382	Z_FLUXERR_APER_15	Error in Z band 24 arcsec diameter circular aperture flux
383	Z_CLASS_STAR	Z band SExtractor classification statistic
384	Ks_DET_FLAG	Ks band Detection flag
385	H_DET_FLAG	H band Detection flag
386	J_DET_FLAG	J band Detection flag

387	Y_DET_FLAG	Y band Detection flag
388	Z_DET_FLAG	Z band Detection flag
389	HALOFLAG	Flag from Halo image

Table 9. Complete list of supplied catalogue columns for the sources lists released with the individual stacked paw-prints and tiles.

No	Name	Column Description
1	Seq No.	Running number for ease of reference, in strict order of image detections
2	Isophotal flux	Standard definition of summed flux within detection isophote, apart from detection filter is used to define pixel connectivity and hence which pixels to include. This helps to reduce edge effects for all isophotally derived parameters.
3	X coord	Intensity–weighted isophotal centre–of–gravity in X
4	Error in X	Estimate of centroid error
5	Y coord	Intensity–weighted isophotal centre–of–gravity in Y
6	Error in Y	Estimate of centroid error
7	Gaussian sigma	These are derived from the three general intensity–weighted second moments
8	Ellipticity	The equivalence between them and a generalised elliptical Gaussian
9	Position angle	Position angle of the isophote
10-17	Areal profile 1-8	Number of pixels above a series of threshold levels relative to local sky. Levels are set at T, 2T, 4T, 8T . . . 128T where T is the threshold. These can be thought of as a radial profile. Note that for now, deblended, i.e. overlapping images, only the first areal profile is computed and the rest are set to –1 flagging the difficulty of computing accurate profiles for blended images this parameter is used to flag the start of the sequence of the deblended components by setting the first in the sequence to 0.
18	Peak height	In counts relative to local value of sky - also zeroth order aperture flux
19	Error in pkht	Error in Peak Height
20-45	Aperture flux 1-13 and error on aperture flux 1-13	These are a series of different radii soft-edged apertures designed to adequately sample the curve-of-growth of the majority of images and to provide fixed-sized aperture fluxes for all images. The scale size for these apertures is selected by defining a scale radius _<FWHM> for site+instrument. In the case of VIRCAM this "core" radius (rcore) has been fixed at 1.0 arcsec for convenience in inter-comparison with other datasets. A 1.0 arcsec radius is equivalent to 3.0 pixels for normal data. In 0.8 arcsec seeing an rcore-radius aperture contains roughly 75% of the total flux of stellar images. The aperture fluxes are sky-corrected integrals (summations) with a soft-edge (i.e. pro-rata flux division for boundary pixels). However, for overlapping images they are more subtle than this since they are in practice simultaneously fitted top-hat functions, to minimise the effects of crowding. Images external to the blend are also flagged and not included in the large radius summations. Starting with parameter 20 the radii are: 1/2× rcore, 1/sqrt(2)× rcore, rcore, sqrt(2)× rcore, 2× rcore, 2sqrt(2)× rcore, 4× rcore, 5× rcore, 6× rcore, 7× rcore, 8× rcore, 10× rcore, 12× rcore We recommend using Aperture flux 3 if a single number is required to represent the flux for ALL images - this aperture has a radius of rcore = 1 arcsec.
46	Petrosian radius	Petrosian radius as defined in Yasuda et al. 2001 AJ 112 1104
47	Kron radius	Kron radius as defined in Bertin and Arnouts 1996 A&A Supp 117 393
48	Hall radius	Hall image scale radius e.g. Hall & Mackay 1984 MNRAS 210 979
49	Petrosian flux	Petrosian flux within circular aperture to k x rp with k=2
50	Error in flux	Error on Petrosian flux
51	Kron flux	Flux within circular aperture to k x rk with k=2

52	Error in flux	Error on Kron flux
53	Hall flux	Flux within circular aperture to k x rh with k=5; alternative total flux
54	Error in flux	Error on Hall flux
55	Error bit flag	Bit pattern listing various processing error flags initially set to the no. of bad pixels within aperture of radius "rcore"- note this can be fractional due to soft-edged apertures
56	Sky level	Local interpolated sky level from background tracker
57	Sky rms	Local estimate of variation in sky level around image
58	Av conf	Average confidence level within default rcore aperture useful for spotting spurious outliers in various parameter selection spaces
		The following are accreted after standard catalogue generation
59	RA	Right Ascension in radians (J2000)
60	Dec	Declination in radians(J2000)
61	Classification	Flag indicating most probable morphological classification: e.g. –1 stellar, +1 non–stellar, 0 noise, –2 borderline stellar (Saturated images can be flagged by comparing the peak height + local sky with the SATURATE keyword in the header.)
62	Statistic	An equivalent N(0,1) measure of how stellar–like an image is, used in deriving parameter 61 in a 'necessary but not sufficient' sense. Derived mainly from the curve-of-growth of flux using the well-defined stellar locus as a function of magnitude as a benchmark (see Irwin et al. 1994 SPIE 5493 411 for more details).
63	MJDoff	The number of minutes to be added to MJD_DAY in order to get the MJD of a given object. Hence for the *i*th object: MJDi = MJD_DAY + MJDoffi /1440.0 (not present in stacked paw-prints or tiles)
64	Blank	Blank
65	Blank	Blank
66	Blank	Blank
67	Blank	Blank
68	Blank	Blank
69	Blank	Blank
70	Blank	Blank
71	Blank	Blank
72	Blank	Blank
73	Blank	Blank
74	Blank	Blank
75	Blank	Blank
76	Blank	Blank
77	Blank	Blank
78	Blank	Blank
79	Blank	Blank
80	Blank	Blank

Acknowledgements

The VIDEO Survey is described in Jarvis et al. 2013, MNRAS, 428, 1281 and any publications using the VIDEO data should reference this article and this DR note.

Please use the following statement in your articles when using these data:
Based on data products from observations made with ESO Telescopes at the La Silla Paranal Observatory as part of the VISTA Deep Extragalactic Observations (VIDEO) survey, under programme ID 179.A-2006 (PI: Jarvis).

References

Bertin E. & Arnouts S., 1996, ApJS, 117, 393
Bertin E., et al., 2002, ASPC, 281, 228
Cross et al. 2012, A&A, 548A, 119
González-Fernandéz, et al., 2018, MNRAS, 474, 5459
Irwin M.J., et al., 2004, SPIE, 5493, 411
Jarvis M.J., et al., 2013, MNRAS, 428, 1281
Schlegel D.J., Finkbeiner D.P. & Davis M., 1998, ApJ, 500, 525
Skrutskie M.F., et al., 2996, AJ, 131, 1163